Science of the Total Environment 645 (2018) 937–945

Contents lists available at ScienceDirect

Science of the Total Environment

journal homepage: www.elsevier.com/locate/scitotenv

Immobilization of powdery calcium silicate hydrate via PVA covalent cross-linking process for phosphorus removal

Shilin Ding [a], Dexin Fang [a], Zishan Pang [b], Bin Luo [b], Li Kuang [c], Han Wang [a], Qian Zhang [a], Qiushi Shen [a], Fangying Ji [a,*]

[a] Key Laboratory of Three Gorges Reservoir Region's Eco-Environment, Ministry of Education, Chongqing University, Chongqing 400045, China
[b] Chongqing Yuxi Water Co., Ltd, Chongqing 402160, China
[c] Chongqing Gangli Environmental Protection Co., Ltd, Chongqing 404100, China

HIGHLIGHTS

- A novel immobilized sheet material was prepared for phosphorous removal.
- The immobilized material reduced the loss of CSH powder during continuous operation.
- The PVA-CSH performance was evaluated by the turbidity and phosphorous concentration.
- The reaction process of phosphorous adsorbed by PVA-CSH was proposed.

GRAPHICAL ABSTRACT

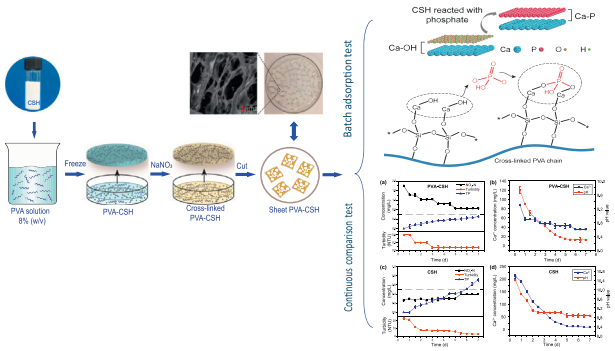

ARTICLE INFO

Article history:
Received 23 May 2018
Received in revised form 15 July 2018
Accepted 15 July 2018
Available online xxxx

Editor: Zhen (Jason) He

Keywords:
Immobilization
Calcium silicate hydrate
Covalent cross-linking
Phosphorus removal
Effluent turbidity

ABSTRACT

Calcium silicate hydrate (CSH) is a popular material used for phosphorus removal in recent years. In this work, a novel immobilized material, polyvinyl alcohol-CSH (PVA-CSH), was prepared using a 1:10 weight ratio of CSH powder to 8% PVA solution and then used for phosphorus removal. Samples were characterized by scanning electron microscopy (SEM), energy dispersive spectroscopy (EDS), X-ray diffraction (XRD) and Fourier transform infrared spectroscopy (FTIR). The adsorption mechanism and practical application properties of phosphorus wastewater were studied by sequential batch and continuous flow experiment. The results showed PVA-CSH possessed a porous network structure and an average pore diameter of 24.94 ± 0.11 nm. Furthermore, the CSH functional groups were unaffected by PVA immobilization. Compared with CSH, PVA-CSH did not easily lose CSH after being immobilized by PVA, and the duration of efficient phosphorus removal stage was approximately 20 h longer than that of CSH. In addition, the effluent turbidity of PVA-CSH was 0.11 ± 0.03 NTU during the continuous operation period, which was significantly lower than CSH. In summary, this research study demonstrated the significant potential of PVA-CSH for practical phosphorus removal.

1. Introduction

Wastewater from municipal, industrial and agricultural activities contains superfluous phosphorus (Zhou et al., 2012). Excessive phosphorus (P) discharged into water bodies may lead to severe

* Corresponding author.
E-mail address: jfy@cqu.edu.cn (F. Ji).

https://doi.org/10.1016/j.scitotenv.2018.07.197
0048-9697/

eutrophication, which results in the degradation of the water ecosystem and destruction of self-purification capacity (Xiao et al., 2017). Therefore, the removal of phosphorus from wastewater is necessary to meet the discharge limit in controlling eutrophication. In the past several decades, several categories of phosphorus removal methods have been proposed, primarily including biological removal (Geng et al., 2018), chemical precipitation (Qiu et al., 2015) and chemical adsorption (Golder et al., 2006). Among these methods, biological removal methods are advantageous because of their low cost, but the phosphorus concentration of the effluent is easily affected by microbial growth conditions. In light of increasingly stringent phosphorus removal standards, chemical precipitation is a very efficient method. However, chemical precipitation methods usually involve the excess addition of chemicals, which can lead to ecological pollution. Electrochemical induced phosphate precipitation has been proven as an efficient method for phosphorus removal (Lei et al., 2017). Besides, chemical adsorption has become a popular phosphorus removal method because of its simple operation and possible phosphate recovery (Sun et al., 2015; Zheng et al., 2011). Various chemisorption materials have been studied as phosphate adsorbents and include layered double hydroxide (LDH) (Novillo et al., 2014), metal-modified carbon (Cui et al., 2016; Yin et al., 2018) and calcium-based materials (Wang et al., 2018), etc. Particularly, calcium-based materials are advantageous for chemical phosphorus removal because of their simple synthesis, rapid reaction speed and environmental friendliness (Bellier et al., 2006). Previous studies of Ca-based materials mainly focused on apatite (Yagi and Fukushi, 2012), monohydrocalcite (Karageorgiou et al., 2007), calcite (Rejmak et al., 2012) and calcium silicate hydrate (CSH) (Renman and Renman, 2010). Studies have reported that calcium silicate materials could remove phosphate from water via chemisorption processes (Chen et al., 2009). CSH, a common synthetic silicate adsorbent, has been widely used because of its large specific surface area and the unique release capability of Ca^{2+} and OH^{-}. CSH is synthesized using calcium oxide and silicon oxide materials (Guan et al., 2013). Okano et al. (2013) prepared amorphous CSH to treat anaerobic sludge digestion solution and determined the phosphate adsorption capacity was approximately 40 mg/g for this use. Kuwahara and Yamashita (2017) demonstrated that CSH synthesized from blast furnace slag (BF slag) could be used as a phosphorus removal adsorbent, with a maximum phosphorus adsorption capacity 73-fold greater than that of BF slag.

Many research studies have demonstrated CSH possesses excellent adsorption properties. However, most synthetic phosphorus removal adsorbents, including CSH, are used as a powder with a particle size ≤100 μm (Bai et al., 2009); CSH can be lost to the effluent because of their small particle size, which decreased the utilization efficiency of adsorbent materials and polluted the environment (Mohan and Pittman Jr, 2007; Okano et al., 2015). Therefore, the development of a method for the suitable immobilization of phosphorus-removing powders is an urgent need. Polyvinyl alcohol (PVA) has been considered a promising immobilization carrier in recent years because of its chemical stability, high mechanical strength and non-toxicity (Takei et al., 2011; Zain et al., 2011).

Chemical cross-linking is the most commonly used method in PVA immobilization, which involves generating a covalent bond between the hydroxyl group of PVA and the functional groups of cross-linking agents (Derwinska et al., 2008; Yujian et al., 2006). Kumar et al. (2009) prepared cross-linked chitosan/PVA beads using an aqueous suspension of chitosan-PVA. Subsequently, the immobilized material was effectively utilized for the removal of Cd (II) ions. Lai et al. (2016) synthesized PVA-alginate granules using boric acid and calcium chloride as cross-linking agents to immobilize Prussian blue nanoparticles for the removal of cesium. Saturated boric acid is one of the most commonly used cross-linking agents. Unfortunately, it still possesses several deficiencies, including its toxicity and swelling properties (Hsia et al., 2008; Zhang et al., 2007). In addition to saturated boric acid, sodium nitrate ($NaNO_3$) has also been developed as a cross-linking agent due to its rapid cross-linking rate and non-toxicity (Hu and Yang, 2014). Materials prepared with $NaNO_3$ exhibited excellent mechanical strength and chemical stability (Chang and Tseng, 1998). The effective immobilization of CSH powder by PVA may reduce the loss of CSH powder during phosphorus removal. However, to our knowledge, no research has been conducted on the use of PVA to immobilize CSH powder.

In the present paper, we immobilized CSH powder with PVA using $NaNO_3$ as the cross-linking agent. Combined with the characterization of PVA-CSH and the recovered product, a possible phosphate removal process by the PVA-CSH was proposed. The focus of this study was to evaluate the phosphorus removal performance of an immobilized material (PVA-CSH) by monitoring effluent turbidity and phosphorus concentration.

2. Materials and methods

2.1. Raw materials

In this study, all materials used were at least analytical purity. CSH powder (80–100 mesh) and PVA (nominal degree of polymerization, 1750 ± 50) were obtained from Shanghai Chemical Reagent Co., Ltd. $NaNO_3$ and KH_2PO_4 were purchased from Chongqing Boyi Chemical Reagent Co., Ltd. These materials and chemicals were stored in sealed bottles. The phosphate solution was prepared by adding KH_2PO_4 into the solution with initial phosphate concentration of 400 mg/L.

2.2. Preparation of PVA-CSH

The preparation of PVA-CSH was performed using four major steps, which are outlined in Fig. 1(a). Step 1: Firstly, an 8% (w/w) aqueous PVA solution was prepared. Secondly, CSH powder was added to the solution using a 1:10 weight ratio of CSH powder to PVA solution. Thirdly, the suspension was subjected to agitation for 15 min. Step 2: Firstly, the evenly dispersed mixture was plated onto a Petri dish. Secondly, the mixture was incubated at −20 °C for 1 h to freeze the mixture into a molded thin sheet with a resulting thickness of 0.5–1.5 mm. Step 3: A 25% (w/v) $NaNO_3$ solution was added to the frozen PVA-CSH sheet. In the next 2 h, the PVA cross-linking reaction will occur via N—O covalent bonds. The proposed PVA cross-linking reaction process using $NaNO_3$ is shown in Fig. 1(b). Step 4: Firstly, the cross-linked sheet material (PVA-CSH) was washed three times with ultrapure water to remove $NaNO_3$ and unbound CSH powder. Secondly, the cross-linked PVA-CSH sheet was trimmed into smaller irregular sheets, which were approximately 1 cm×1 cm in size. Additionally, the reaction process of PVA and CSH is shown in Fig. 1(c).

2.3. Characterization of PVA-CSH

Scanning electron microscopy (SEM) and energy dispersive spectroscopy (EDS) analyses of the prepared material (PVA-CSH) were performed with a JSM-7800F SEM (Electronics JEOL Corp., Japan). Nitrogen adsorption-desorption isotherms were measured by a nitrogen adsorption apparatus (ASAP2020, Micromeritics Corp., USA). Specific surface areas were calculated using the Brunauer-Emmett-Teller (BET) method, and pore sizes were obtained from the adsorption branch of nitrogen isotherms using the Barrett-Joyner-Halenda (BJH) method. The phase composition of PVA-CSH and CSH before and after reacting with phosphate was examined by X-ray diffraction (XRD, Thermo Fisher Scientific, China). The chemical bonds present in samples were determined by Fourier transform infrared spectroscopy (FTIR, Shimadzu, Japan) over a range of 400–4000 cm^{-1}.

2.4. Solubility experiments

The release of Ca^{2+} from PVA-CSH and CSH was investigated via a series of batch experiments. For each experiment, 0.68 g of PVS-CSH

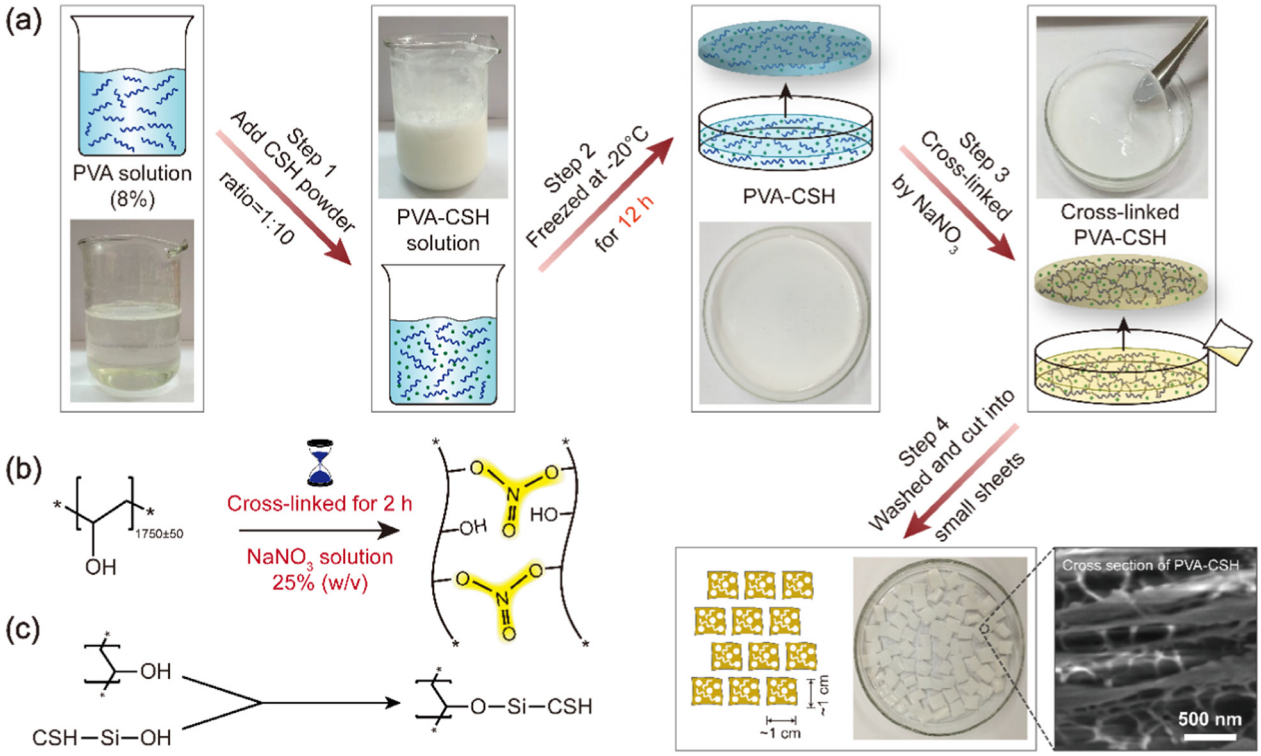

Fig. 1. (a) Synthetic pathway of the formation of PVA-CSH sheets and micrograph of the porous net structure formed, (b) the proposed PVA cross-linking reaction using $NaNO_3$ and (c) the reaction process between PVA and CSH.

(containing 0.40 g CSH) and 0.40 g CSH were mixed with 200 mL ultrapure water (18.24 MΩ·cm) in glass bottles. The bottles were then placed on an agitation table and mixed at 40 rpm at 298 K for 5, 10, 20, 40, 60, 80 and 100 min. The resulting Ca^{2+} concentration was determined by Inductively Coupled Plasma Optical Emission Spectrometer (ICP-OES, iCAP 6300 Duo, Thermo Fisher, USA).

2.5. Adsorption studies

2.5.1. Batch adsorption experiments

All batch adsorption experiments were performed by water bath shaker set to 298 K, adjusting different concentrations of phosphorus-containing wastewater to the same initial conditions (pH = 7.50) by adding sodium hydroxide solution (NaOH, 1.00 mol/L) and hydrochloric acid (HCl, 1.00 mol/L). For the adsorption kinetics, 0.34 g prepared PVA-CSH (containing 0.20 g CSH) and 0.20 g CSH powder were added to two separate conical flasks. Subsequently, 100 mL phosphorus-containing wastewater (20 mg/L) was added to each conical flask. Samples were taken from both flasks every 30 min to monitor the phosphorus content. For adsorption isotherms, 0.68 g prepared PVA-CSH (containing 0.40 g CSH) and 0.40 g CSH powder were added to two separate conical flasks. Subsequently, 100 mL phosphorus-containing wastewater with different initial concentrations (5, 20, 45, 70, 100 and 120 mg/L) was added to the conical flasks. At the end of the adsorption period, suspensions were filtered through a 0.45 μm cellulose acetate membrane (Hens and Merckx, 2002). The phosphate concentration present in the filtrate was measured via molybdate spectrophotometry and UV–vis spectroscopy (Shimadzu Corp., Japan). In addition, the solution pH was measured using a PHS-3C pH meter (Leici Instruments, China).

All experiments were repeated three times, and the average values of these three experiments were calculated. The equilibrium adsorption capacity (q_e) was determined using Eq. (1) (Zhao et al., 2016):

$$q_e = (C_0 - C_e) \times \frac{V}{m} \quad (1)$$

where C_0 and C_e (mg/L) represent the concentration of phosphorus under initial and equilibrium conditions, respectively; V (L) represents the volume of the test solution; and m (g) represents the mass of the adsorbent (PVA-CSH or CSH) used.

2.5.2. Continuous flow phosphorus removal experiment

The two indicators of effluent phosphorus concentration and turbidity were used to comprehensively evaluate the practical performance of

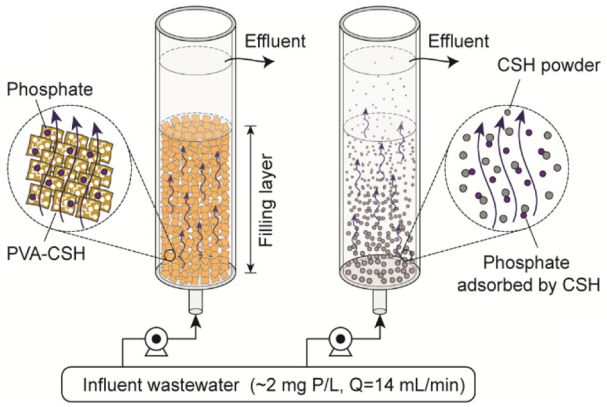

Fig. 2. Continuous flow device for phosphorus removal using PVA-CSH and CSH powder.

phosphorus removal of the immobilized CSH (PVA-CSH) and CSH powder. On the other hand, PVA-CSH was prepared with $NaNO_3$ as the cross-linking agent and the NO_3-N concentration in the effluent was also an important indicator to evaluate the material properties. The dynamic phosphorus removal experimental device is shown in Fig. 2. Added 68 g PVA-CSH (contain 40 g CSH) and 40 g CSH powder into two identical plexiglass columns ($\Phi 32 \times 400$ mm, V = 280 mL, hydraulic loading = 1.70 $cm^3/cm^2 \cdot min$). Under the continuous inflow operation (C_0 = 2 mg P/L, Q = 14 mL/min, HRT = 20 min, phosphate loading rate = 1.00 mg P/g CSH·d), samples were taken every 2 h to monitor changes in phosphorus concentration and NO_3-N concentration in the effluent. In addition, the effluent turbidity was analyzed using a HACH 2100q portable turbidimeter (HACH Corp., USA). When the phosphorus concentration reached the breakthrough point (>0.5 mg/L), wastewater treatment was terminated and the termination time was recorded.

3. Results and discussion

3.1. Characterization of PVA-CSH

3.1.1. SEM analysis

SEM images of the fresh PVA-CSH surface and cross-section are shown in Fig. 3(a) and (b). PVA-CSH was network-like with large pores, numerous folds and an irregular shape. The open framework structure indicated PVA-CSH had a large pore volume, which could be

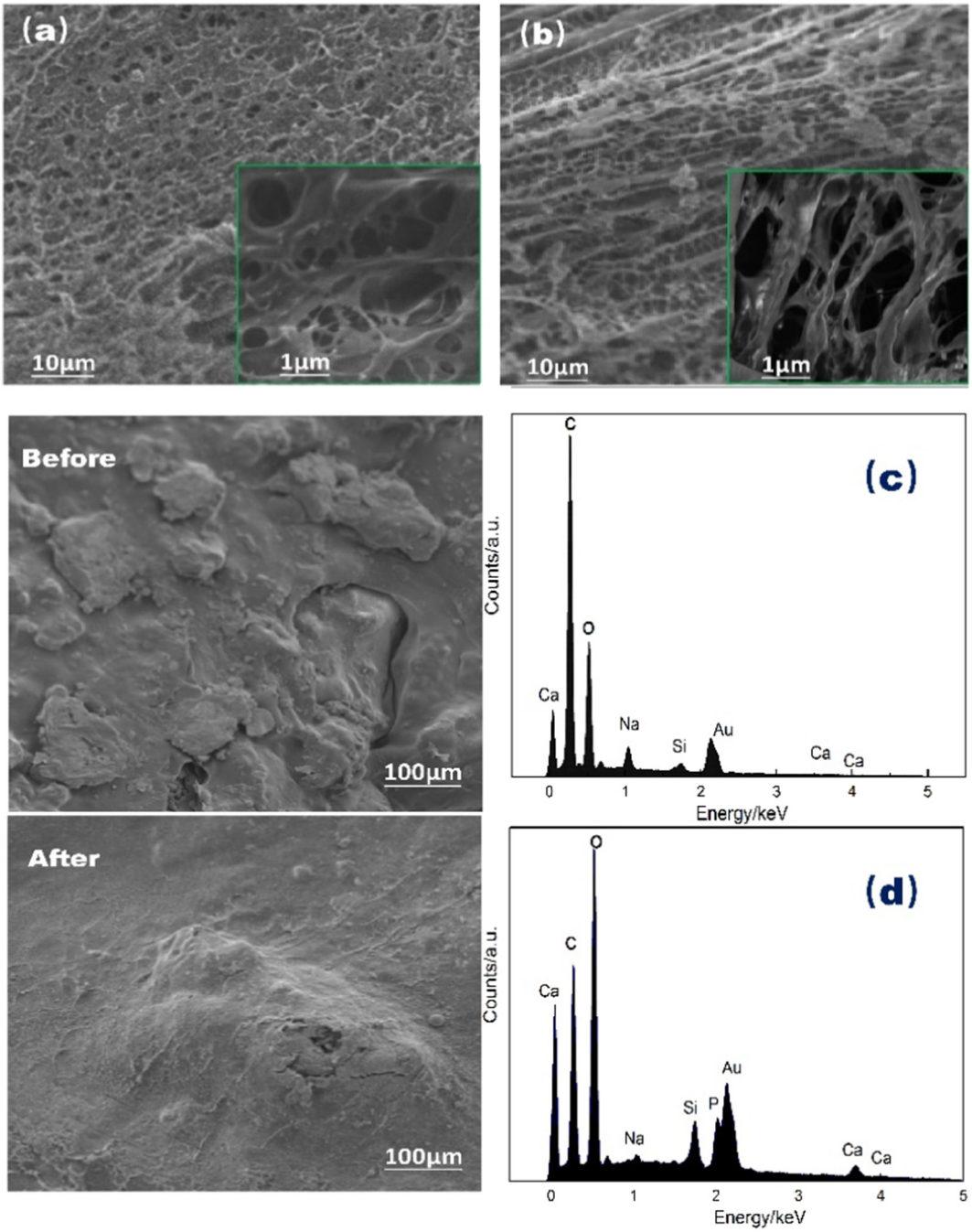

Fig. 3. Changes in surface microstructure and elemental composition of PVA-CSH: (a) SEM image of surface, (b) SEM image of cross-section, SEM images and EDS analysis results before (c) and after (d) reaction with phosphate.

Table 1
BET specific surface area and pore structure parameters of PVA-CSH and CSH.

Sample	Specific surface area (m^2/g)	Total pore volume (cm^3/g)	Peak pore diameter (nm)	Pore diameter range (nm)
PVA-CSH	4.123	0.011	24.937	1.700–300
CSH	20.217	0.034	13.121	0.080–112

beneficial for adsorbates that were readily accessible (Kuwahara et al., 2013). In addition, the microstructure data of the PVA-CSH and CSH samples are shown in Table 1. Compared with CSH, the pore distributions indicated that the PVA-CSH had lager peak pore diameter pores with an average of 24.937 nm. The result proved that porous structure of CSH powder was not destroyed by the PVA immobilization. The abundant and larger diameter pores might provide more Ca^{2+} reactive binding sites for adsorpting phosphate. Furthermore, the sheet structure of PVA-CSH could provide increased free access to ions because of comparatively shorter distances between molecules.

3.1.2. EDS analysis

The SEM photographs and corresponding EDS spectra (c, d) of PVA-CSH before and after phosphorus adsorption experiments are presented in Fig. 3. The presence of phosphorus (3.75%) in the EDS spectrum indicated that phosphate has been adsorbed to the PVA-CSH. Compared with fresh PVA-CSH, it can be clearly seen that the folded structure of PVA-CSH became smoother, revealing that the porous structure disappeared after reacting with phosphate. Calcium-based materials have already demonstrated their potential to bind phosphate ions from wastewater: a strong affinity exists between Ca^{2+} and phosphate ions and results in the formation of an insoluble calcium phosphate species (Gustafsson et al., 2008; Yin et al., 2011). These results indicated phosphate could be removed from wastewater by PVA-CSH.

3.1.3. XRD analysis

XRD analysis was performed to observe the phase composition of PVA-CSH and CSH before and after reaction with phosphate; the XRD patterns are shown in Fig. 4. The major phase of fresh CSH and PVA-CSH was Jennite (PDF card 18–1206, $Ca_9Si_6O_{18}(OH)_6{\cdot}8H_2O$). Additionally, peaks located at $2\theta = 23.1°$, 36.0°, 39.4°, 43.2° and 48.5° corresponded to calcite (PDF card 47-1743). Calcite formation was caused by inevitable contact with atmospheric carbon dioxide during the preparation of PVA-CSH and CSH. Besides, the peak at $2\theta = 19.68°$ correspond to the monoclinic unit cell of PVA (Lauprêtre et al., 2004).

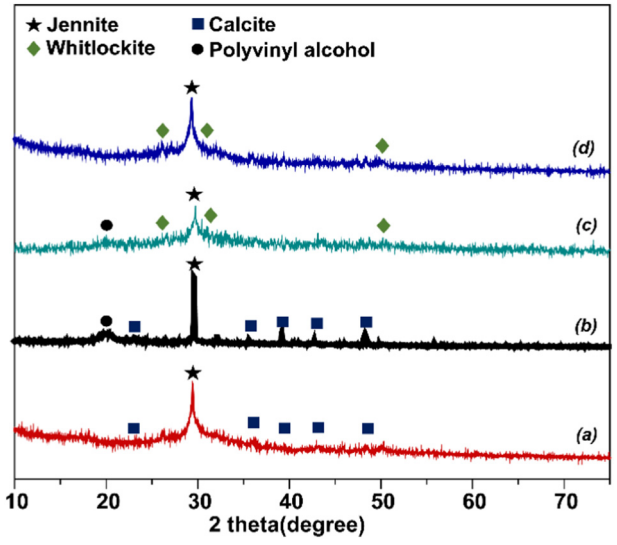

Fig. 4. XRD patterns of PVA-CSH and CSH samples before (b) (c) and after (a) (d) reaction with phosphate.

After the reaction, the sharp and dominant reflection of whitlockite (PDF card 09-0169, $Ca_3(PO_4)_2$) appeared at $2\theta = 26.5°$, 30.9° and 50.1°, indicating that soluble phosphate was primarily composed of $Ca_3(PO_4)_2$.

3.1.4. FTIR analysis

FTIR was used to further identify the functional groups and chemical compositions of fresh CSH, PVA and PVA-CSH (Fig. 5). The three samples showed broad peaks at 3440 cm^{-1} and 1638 cm^{-1}, which were attributed to the bending vibration of —OH (Guan et al., 2013; Zhang and Chang, 2010). The characteristic peaks of PVA located at 1390 cm^{-1} were ascribed to the bending vibration of the C—H group. In addition, the peaks located at approximately 970 cm^{-1} and 660 cm^{-1} were attributed to the stretching vibration of O—Si—O and the bending vibration of Si—O—Si, respectively. These bands embody the unique silicon oxygen tetrahedral structure of CSH (Guan and Zhao, 2016; Mostafa et al., 2009). These results showed the functional groups and chemical composition of CSH were retained after PVA immobilization. After the phosphorus adsorption reaction, the strength of absorption peaks at 3440 cm^{-1} and 1638 cm^{-1} become weak. Additionally, the peaks at 570 cm^{-1} and 1440 cm^{-1} corresponded to phosphate, indicating that the phosphate present in the wastewater had been bound effectively by PVA-CSH and CSH. These results demonstrated that the surface Ca-OH groups played a key role in phosphate ion exchange.

3.2. A proposed phosphate removal process for PVA-CSH

The Ca^{2+} released, and changes of pH during batch adsorption process were presented in Fig. 6 (a) and (b), respectively. CSH (4.98 mg/g CSH) exhibited a nearly identical Ca^{2+} release capacity compared with PVA-CSH (4.32 mg/g CSH). Correspondingly, the Ca^{2+} release rate of PVA-CSH was slightly slower than that of CSH, which might be due to the release of Ca^{2+} being delayed by PVA immobilization. Nevertheless, large amounts of Ca^{2+} and OH^- from PVA-CSH were released into the water spontaneously. Besides, phosphate ions were concentrated on the surface of PVA-CSH and reacted with Ca-OH groups, as reflected by FTIR spectra. When the reaction was conducted for 180 min, the pH was close to equilibrium, indicating that OH^- ions were consumed in the process of forming calcium phosphate, and the equilibrium pH of PVA-CSH and CSH were 9.61 and 9.31, respectively. This result seemed to suggest that the soluble phosphate was mainly composed of $Ca_3(PO_4)_2$, which was confirmed by XRD.

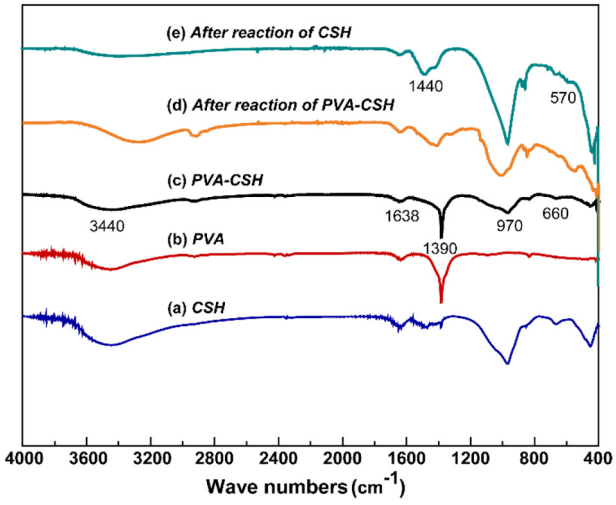

Fig. 5. Structural characterization before and after reaction with phosphate: (a) CSH, (b) PVA and (c) PVA-CSH are FTIR spectra before reaction with phosphate; (d) PVA-CSH and (e) CSH are FTIR spectra after reaction with phosphate.

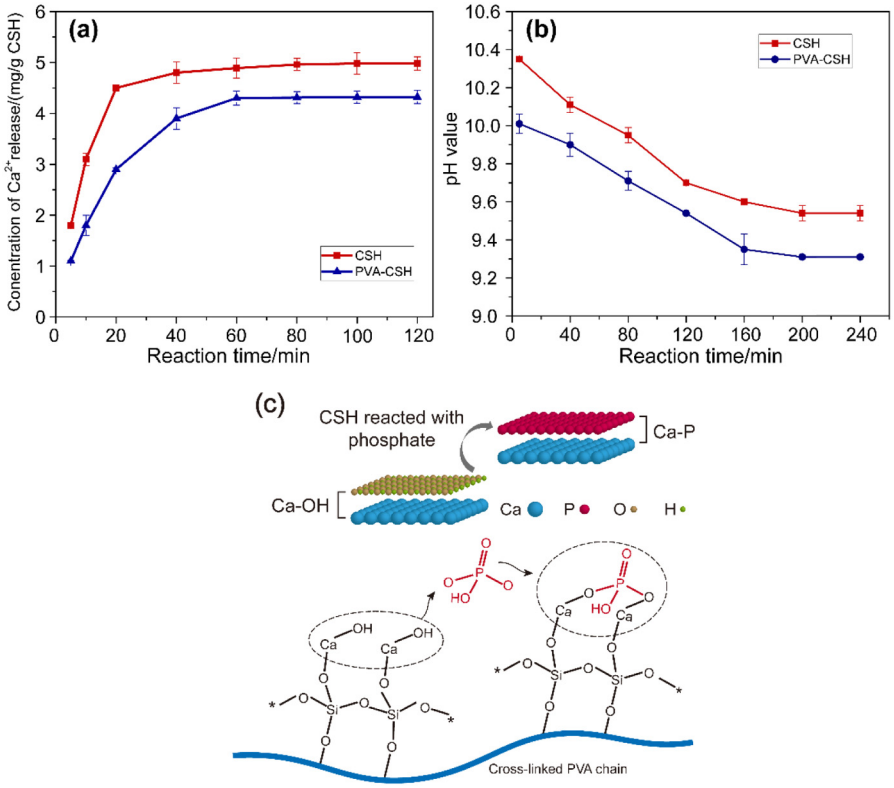

Fig. 6. (a)Variations in the concentration of Ca^{2+} released from CSH samples in ultra-pure water, (b) change in the pH during the batch adsorption process and (c) the proposed phosphate removal process of PVA-CSH.

Based on the previous analyses, a proposed phosphorus adsorption process by PVA-CSH is shown in Fig. 6(c). The phosphate removal process can be described as follows: (1) the phosphate was concentrated on and became attracted to the surface or the surrounding area of PVA-CSH, and Ca^{2+} was spontaneously released from the CSH surface and reacted with PO_4^{3-}, forming $Ca_3(PO4)_2$; (2) Ca-OH linkages on the surface of PVA-CSH reacting with phosphate through ion exchange with OH^- to form calcium phosphate.

3.3. Kinetic studies

The experimental data of the kinetic study were fitted to pseudo-first-order and pseudo-second-order models, which are presented in Eqs. (2) and (3), respectively:

$$\log(q_0 - q_e) = \log q_e - \left(\frac{k_1}{2.303}\right)t \tag{2}$$

$$\frac{t}{q_t} = \frac{1}{k_2 q_e^2} + \left(\frac{1}{q_e}\right)t \tag{3}$$

where q_e and q_t (mg P/g) represent the mass of phosphorus adsorbed per unit mass of adsorbent at equilibrium and at specific adsorption time t (min), respectively, and k_1 (1/min) and k_2 (g/(mg min)) are the rate constants of the pseudo-first-order and pseudo-second-order models, respectively.

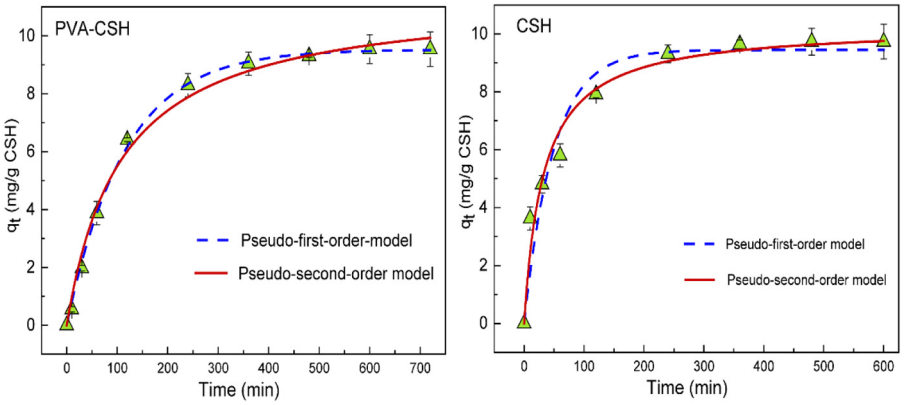

Fig. 7. Dynamic nonlinear fitting curve and experimental adsorption data of PVA-CSH and CSH.

The adsorption kinetic curves of PVA-CSH and CSH are shown in Fig. 7. The adsorption reaction of the CSH powder had an equilibrium time of 480 min while the equilibrium time of immobilized PVA-CSH was approximately 600 min. The equilibrium time of PVA-CSH was 120 min longer than that of CSH powder. Additionally, for the pseudo-second-order fitting equation, the CSH reaction rate constant ($k_{1,\ CSH} = 0.0030$) of CSH was larger than that of PVA-CSH ($k_{2,\ PVA\text{-}CSH} = 0.0008$). These results might also have occurred because of the decreased surface area caused by the PVA immobilization, which decreased the reaction rate and prolonged the equilibration time. Experimental data showed a better fitting of pseudo-second order model, with higher correlation coefficients ($R^2 = 0.9713$ for PVA-CSH and 0.9913 for CSH), indicating this kinetic model fits the experimental data well. These results revealed phosphorus removal by the PVA-CSH and CSH was a chemical process (Kuwahara et al., 2013). In addition, Li et al. (2015) prepared nanostructured CSH and evaluated the effects of phosphorus adsorption. Their results showed the adsorption process remained in line with the pseudo-second-order kinetic model.

3.4. Adsorption isotherms

The adsorption isotherm data were fit to the following Langmuir and Freundlich equations:

$$\text{Langmuir}: q_e = \frac{bq_m C_e}{1 + bC_e} \tag{4}$$

$$\text{Freundlich}: q_e = kC_e^{1/n} \tag{5}$$

where C_e (mg P/L) represents the equilibrium concentration of phosphorus; q_e (mg P/g) represents the amount of phosphorus adsorbed per unit mass of adsorbent at equilibrium; q_m (mg P/g) is the Langmuir constant that represents maximum adsorption capacity assuming a monolayer coverage of adsorbate over a homogenous adsorbent surface; b is a kinetic parameter representing the adsorption energy of the adsorbent for the adsorbate phosphate; k (mg P/g) is the Freundlich constant related to adsorption capacity; and $1/n$ is an empirical parameter related to adsorption intensity or surface heterogeneity.

The construction of adsorption isotherms was helpful for understanding the mechanism of contaminant adsorption and to predict the maximum equilibrium adsorption capacity of PVA-CSH (Armagan et al., 2003; Sarkar et al., 2010). The adsorption isotherms of PVA-CSH and CSH are presented in Fig. 8. Compared with the Freundlich isotherm model, adsorption data exhibited an excellent fitting of Langmuir isotherm model, with higher correlation coefficient values ($R^2 = 0.9877$ for PVA-CSH and 0.9898 for CSH). These results revealed the adsorption process involves uniform monolayer surface adsorption (Okano et al., 2015). The theoretical maximum adsorption capacities of CSH and PVA-CSH were 31.06 mg/g CSH and 28.15 mg/g CSH, respectively, using isotherm fitting equations. The experimental results showed that the equilibrium adsorption capacities of the CSH powder and immobilized PVA-CSH were 22.95 mg/g CSH and 22.85 mg/g CSH, respectively. The amount of CSH in the PVA-CSH was consistent with the CSH powder, confirming the phosphorus removal performance of PVA-CSH was unaffected by the PVA immobilization, Furthermore, the results confirmed the porous structure of CSH powder remained unchanged. In summary, phosphorus removal using PVA-CSH was demonstrated as feasible.

3.5. Adsorption thermodynamics

The thermodynamic factor was measured by various thermodynamic parameters in which the Gibbs free energy (Devi et al., 2017) change is given by Eq. (6).

$$\Delta G^0 = -RT1\text{n}\ K_c \tag{6}$$

where K_c (L/g) is the standard thermodynamic equilibrium constant, R (8.314 J/mol/K) is the universal gas constant, and T (298 K) represents the reaction temperature.

K_c was calculated using the equilibrium adsorption capacity of the phosphorus concentration according to Eq. (7).

$$K_c = \frac{q_e}{C_e} \tag{7}$$

Based on adsorption kinetics experiments, the equilibrium adsorption capacities of PVA-CSH and CSH were 9.54 mg/g CSH and 9.69 mg/g CSH, respectively. Negative ΔG^0 values of the adsorption reactions of PVA-CSH ($\Delta G^0 = -11.5$ kJ/mol) and CSH powder ($\Delta G^0 = -12.52$ kJ/mol) were calculated using Eqs. (6) and (7), indicating the adsorption processes proceeded spontaneously.

3.6. PVA-CSH and CSH continuous flow comparison experiments

In order to evaluate the practicality of PVA-CSH, a continuous flow device for removing phosphorus was operated for seven days, treating a total wastewater volume of 205 L. As shown in Fig. 9 (a) (c), the effluent turbidity of the CSH column dropped sharply from 23 to 7.5 nephelometric turbidity units (NTU) within the first two days. This result indicated the CSH powder possessed a small particle size, which led to adsorbent loss with the water flow. And it descended slowly from 7.5 NTU to 3 NTU during the next four days, which was attributed to the increasing sedimentation performance of the particles. Compared with CSH, the effluent turbidity of PVA-CSH was 0.11 ± 0.03 NTU during the entire operating period, confirming that the immobilization of CSH to PVA reduced CSH loss and demonstrating PVA-CSH was easily

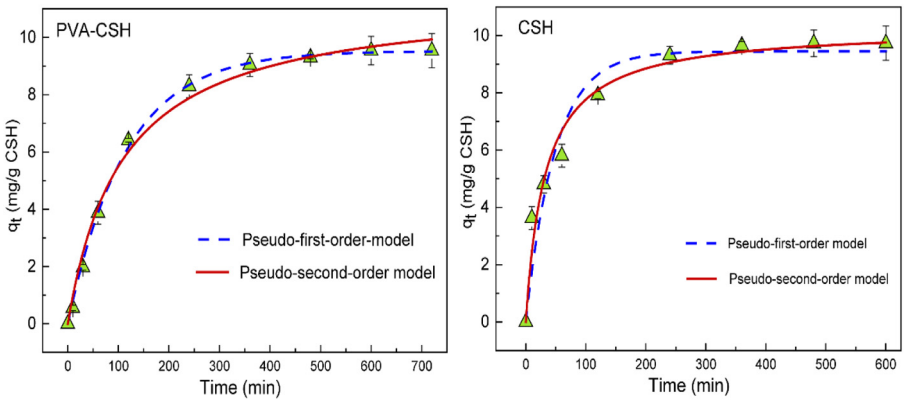

Fig. 8. Nonlinear curve fits of PVA-CSH and CSH adsorption equilibrium data with different adsorption isotherm equations.

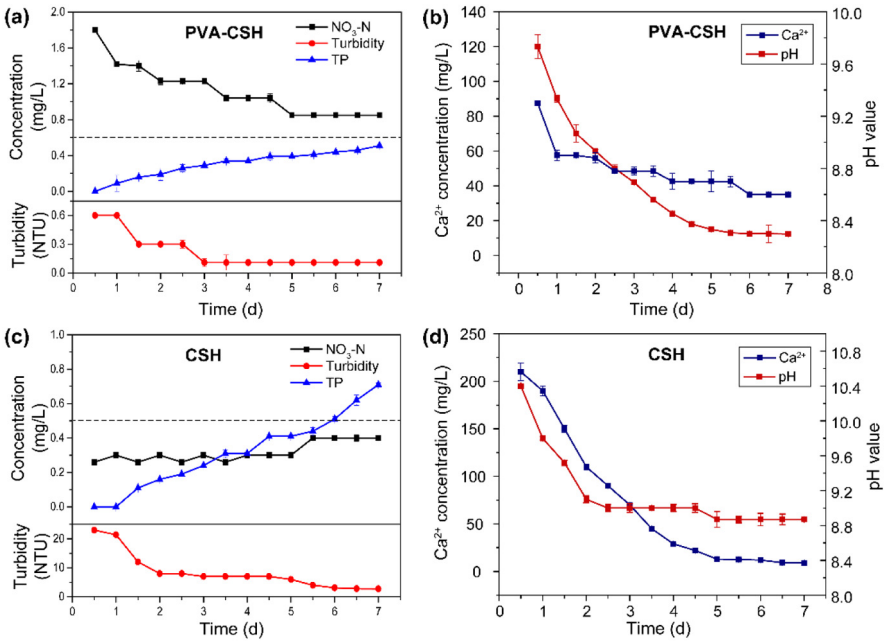

Fig. 9. The change of turbidity, TP, NO_3-N, pH and Ca^{2+} concentration of (a) (b) PVA-CSH and (c) (d) CSH in effluent.

separated from wastewater. Previous studies have suggested that CSH can release Ca^{2+} and OH^- ions to form calcium phosphate by reacting with phosphate (Southam et al., 2008).

As reflected by change of pH value and Ca^{2+} concentration in effluent (Fig. 9 (b) (d)), the pH and Ca^{2+} concentration of CSH were larger than that of PVA-CSH within four days, the result indicated that powdery CSH has a higher ability of release OH^- and Ca^{2+} at initial stage. And it also explained the reason that powdery CSH was more easily lost OH^- and Ca^{2+} than that of PVA-CSH during continuous operation. After the fourth day, the pH value and Ca^{2+} concentration was close to equilibrium, indicating that the ability of CSH to release OH^- and Ca^{2+} ions had reached its utmost. Differently, in addition to the release of OH^- and Ca^{2+}, phosphate ions were also adsorbed to the surface of PVA-CSH react with Ca-OH. The competence of phosphorus removal of PVA-CSH was superior to CSH from the fourth day to seventh day. When the reactor reached the breakthrough point (i.e. effluent TP > 0.5 mg/L), the duration of PVA-CSH (164 h) was approximately 20 h longer than CSH (144 h). Results proved that the PVA-CSH shows a better phosphorus removal performance in practical application. On the other hand, the effluent NO_3-N concentration of PVA-CSH column decreased from its initial concentration, 1.8 mg/L, to 1.0 mg/L within four days. Nitrates that did not fully cross-link with PVA were released during the initial operation stage. However, after the fourth day, the effluent NO_3-N concentration of PVA-CSH column was gradually stabilized at 0.78 mg/L, demonstrating that the PVA-CSH no longer released nitrate when the reactor was running steadily. And it also confirmed that the PVA-CSH shows a certain stability in practical applications. Notably, the effluent NO_3-N concentration of the CSH column, 0.3 mg/L, was consistent with the influent NO_3-N concentration during the course of the operation.

4. Conclusion

In this study, prepared PVA-CSH material with a porous network structure was used to treat phosphorus-containing wastewater. According to the batch experiments, the kinetic process matched the pseudo-second-order model well and isothermal adsorption followed the Langmuir model. The maximum adsorption capacities of CSH (31.06 mg/g CSH) was nearly consistent with PVA-CSH (28.15 mg/g CSH) showed that the PVA-CSH still maintained an efficient phosphorus removal performance. In addition, the Gibbs free energy, $\Delta G^0 < 0$ (−12.52 kJ/mol), for the adsorption reaction of PVA-CSH indicated that the adsorption reaction proceeds spontaneously at 298 K. Furthermore, PVA-CSH achieved the standard of effluent phosphorus concentration (TP < 0.5 mg/L). And effluent turbidity was 0.11 ± 0.03 NTU during the continuous operation period, which was effectively reduced the amount of CSH lost. Therefore, the PVA-CSH has exhibited sufficient potential for use in engineering applications of phosphorus adsorption.

Acknowledgements

This work was supported by the Chongqing Science and Technology Commission [grand number: cstc2017shmsA20007] and graduate research and innovation foundation of Chongqing, China [Grant No. CYB18040].

References

Armagan, B., Ozdemir, O., Turan, M., Celik, M.S., 2003. Adsorption of negatively charged azo dyes onto surfactant-modified sepiolite. J. Environ. Eng. 129, 709–715.
Bai, X., Ye, Z.F., Qu, Y.Z., Li, Y.F., Wang, Z.Y., 2009. Immobilization of nanoscale Fe^0 in and on PVA microspheres for nitrobenzene reduction. J. Hazard. Mater. 172, 1357–1364.
Bellier, N., Chazarenc, F., Comeau, Y., 2006. Phosphorus removal from wastewater by mineral apatite. Water Res. 40, 2965–2971.
Chang, C.C., Tseng, S.K., 1998. Immobilization of Alcaligenes eutrophus using PVA crosslinked with sodium nitrate. Biotechnol. Tech. 12, 865–868.
Chen, X., Kong, H., Wu, D., Wang, X., Lin, Y., 2009. Phosphate removal and recovery through crystallization of hydroxyapatite using xonotlite as seed crystal. J. Environ. Sci. 21, 575–580.
Cui, X., Dai, X., Khan, K.Y., Li, T., Yang, X., He, Z., 2016. Removal of phosphate from aqueous solution using magnesium-alginate/chitosan modified biochar microspheres derived from *Thalia dealbata*. Bioresour. Technol. 218, 1123–1132.
Derwinska, K., Sauer, U., Preininger, C., 2008. Adsorption versus covalent, statistically oriented and covalent, site-specific IgG immobilization on poly(vinyl alcohol)-based surfaces. Talanta 77, 652–658.
Devi, V., Selvaraj, M., Selvam, P., Kumar, A.A., Sankar, S., Dinakaran, K., 2017. Preparation and characterization of CNSR functionalized Fe_3O_4 magnetic nanoparticles: an efficient adsorbent for the removal of cadmium ion from water. J. Environ. Chem. Eng. 5, 4539–4546.
Geng, Y.K., Wang, Y., Pan, X.R., Sheng, G.P., 2018. Electricity generation and in situ phosphate recovery from enhanced biological phosphorus removal sludge by electrodialysis membrane bioreactor. Bioresour. Technol. 247, 471–476.
Golder, A.K., Samanta, A.N., Ray, S., 2006. Removal of phosphate from aqueous solutions using calcined metal hydroxides sludge waste generated from electrocoagulation. Sep. Purif. Technol. 52, 102–109.
Guan, W., Zhao, X., 2016. Fluoride recovery using porous calcium silicate hydrates via spontaneous Ca^{2+} and OH^- release. Sep. Purif. Technol. 165, 71–77.

Guan, W., Ji, F., Chen, Q., Yan, P., Zhang, Q., 2013. Preparation and phosphorus recovery performance of porous calcium–silicate–hydrate. Ceram. Int. 39, 1385–1391.
Gustafsson, J.P., Renman, A., Renman, G., Poll, K., 2008. Phosphate removal by mineral-based sorbents used in filters for small-scale wastewater treatment. Water Res. 42, 189–197.
Hens, M., Merckx, R., 2002. The role of colloidal particles in the speciation and analysis of "dissolved"phosphorus. Water Res. 36, 1483–1492.
Hsia, T.H., Feng, Y.J., Ho, C.M., Chou, W.P., Tseng, S.K., 2008. PVA-alginate immobilized cells for anaerobic ammonium oxidation (anammox) process. J. Ind. Microbiol. Biotechnol. 35, 721–727.
Hu, J., Yang, Q., 2014. Microbial degradation of di-n-butyl phthalate by Micrococcus sp. immobilized with polyvinyl alcohol. Desalin. Water Treat. 56, 2457–2463.
Karageorgiou, K., Paschalis, M., Anastassakis, G.N., 2007. Removal of phosphate species from solution by adsorption onto calcite used as natural adsorbent. J. Hazard. Mater. 139, 447–452.
Kumar, M., Tripathi, B.P., Shahi, V.K., 2009. Crosslinked chitosan/polyvinyl alcohol blend beads for removal and recovery of Cd(II) from wastewater. J. Hazard. Mater. 172, 1041–1048.
Kuwahara, Y., Yamashita, H., 2017. Phosphate removal from aqueous solutions using calcium silicate hydrate prepared from blast furnace slag. ISIJ Int. 57, 1657–1664.
Kuwahara, Y., Tamagawa, S., Fujitani, T., Yamashita, H., 2013. A novel conversion process for waste slag: synthesis of calcium silicate hydrate from blast furnace slag and its application as a versatile adsorbent for water purification. J. Mater. Chem. A 1, 7199.
Lai, Y.C., Chang, Y.R., Chen, M.L., Lo, Y.K., Lai, J.Y., Lee, D.J., 2016. Poly(vinyl alcohol) and alginate cross-linked matrix with immobilized Prussian blue and ion exchange resin for cesium removal from waters. Bioresour. Technol. 214, 192–198.
Lauprêtre, F., Ricciardi, R., Auriemma, F., De Rosa, C., 2004. X-ray diffraction analysis of poly(vinyl alcohol) hydrogels, obtained by freezing and thawing techniques. Macromolecules 37, 1921–1927.
Lei, Y., Song, B., van der Weijden, R.D., Saakes, M., Buisman, C.J.N., 2017. Electrochemical induced calcium phosphate precipitation: importance of local pH. Environ. Sci. Technol. 51, 11156–11164.
Li, C.-x., Zhong, H., Wang, S., J-r, Xue, F-f, Wu, Z-y, Zhang, 2015. Preparation of MnO_2 and calcium silicate hydrate from electrolytic manganese residue and evaluation of adsorption properties. J. Cent. South Univ. 22, 2493–2502.
Mohan, D., Pittman Jr., C.U., 2007. Arsenic removal from water/wastewater using adsorbents—a critical review. J. Hazard. Mater. 142, 1–53.
Mostafa, N.Y., Kishar, E.A., Abo-El-Enein, S.A., 2009. FTIR study and cation exchange capacity of Fe^{3+}- and Mg^{2+}-substituted calcium silicate hydrates. J. Alloys Compd. 473, 538–542.
Novillo, C., Guaya, D., Allen-Perkins Avendaño, A., Armijos, C., Cortina, J.L., Cota, I., 2014. Evaluation of phosphate removal capacity of mg/Al layered double hydroxides from aqueous solutions. Fuel 138, 72–79.
Okano, K., Uemoto, M., Kagami, J., Miura, K., Aketo, T., Toda, M., et al., 2013. Novel technique for phosphorus recovery from aqueous solutions using amorphous calcium silicate hydrates (A-CSHs). Water Res. 47, 2251–2259.
Okano, K., Miyamaru, S., Kitao, A., Takano, H., Aketo, T., Toda, M., et al., 2015. Amorphous calcium silicate hydrates and their possible mechanism for recovering phosphate from wastewater. Sep. Purif. Technol. 144, 63–69.
Qiu, L., Zheng, P., Zhang, M., Yu, X., Abbas, G., 2015. Phosphorus removal using ferric–calcium complex as precipitant: parameters optimization and phosphorus-recycling potential. Chem. Eng. J. 268, 230–235.
Rejmak, P., Dolado, J.S., Stott, M.J., Ayuela, A., 2012. 29Si NMR in cement: a theoretical study on calcium silicate hydrates. J. Phys. Chem. C 116, 9755–9761.
Renman, A., Renman, G., 2010. Long-term phosphate removal by the calcium-silicate material Polonite in wastewater filtration systems. Chemosphere 79, 659–664.
Sarkar, B., Xi, Y., Megharaj, M., Krishnamurti, G.S., Naidu, R., 2010. Synthesis and characterisation of novel organopalygorskites for removal of p-nitrophenol from aqueous solution: isothermal studies. J. Colloid Interface Sci. 350, 295–304.
Southam, D.C., Lewis, T.W., McFarlane, A.J., Borrmann, T., Johnston, J.H., 2008. Calcium-phosphorus interactions at a nano-structured silicate surface. J. Colloid Interface Sci. 319, 489–497.
Sun, J., Li, X., Quan, Y., Yin, Y., Zheng, S., 2015. Effect of long-term organic removal on ion exchange properties and performance during sewage tertiary treatment by conventional anion exchange resins. Chemosphere 136, 181–189.
Takei, T., Ikeda, K., Ijima, H., Kawakami, K., 2011. Fabrication of poly(vinyl alcohol) hydrogel beads crosslinked using sodium sulfate for microorganism immobilization. Process Biochem. 46, 566–571.
Wang, S., Kong, L., Long, J., Su, M., Diao, Z., Chang, X., et al., 2018. Adsorption of phosphorus by calcium-flour biochar: isotherm, kinetic and transformation studies. Chemosphere 195, 666–672.
Xiao, X., Liu, S., Zhang, X., Zheng, S., 2017. Phosphorus removal and recovery from secondary effluent in sewage treatment plant by magnetite mineral microparticles. Powder Technol. 306, 68–73.
Yagi, S., Fukushi, K., 2012. Removal of phosphate from solution by adsorption and precipitation of calcium phosphate onto monohydrocalcite. J. Colloid Interface Sci. 384, 128–136.
Yin, H., Yun, Y., Zhang, Y., Fan, C., 2011. Phosphate removal from wastewaters by a naturally occurring, calcium-rich sepiolite. J. Hazard. Mater. 198, 362–369.
Yin, Q., Wang, R., Zhao, Z., 2018. Application of Mg–Al-modified biochar for simultaneous removal of ammonium, nitrate, and phosphate from eutrophic water. J. Clean. Prod. 176, 230–240.
Yujian, W., Xiaojuan, Y., Hongyu, L., Wei, T., 2006. Immobilization of *Acidithiobacillus ferrooxidans* with complex of PVA and sodium alginate. Polym. Degrad. Stab. 91, 2408–2414.
Zain, N.A.M., Suhaimi, M.S., Idris, A., 2011. Development and modification of PVA–alginate as a suitable immobilization matrix. Process Biochem. 46, 2122–2129.
Zhang, M., Chang, J., 2010. Surfactant-assisted sonochemical synthesis of hollow calcium silicate hydrate (CSH) microspheres for drug delivery. Ultrason. Sonochem. 17, 789–792.
Zhang, L.-s., Wu, W.-z., Wang, J.-l., 2007. Immobilization of activated sludge using improved polyvinyl alcohol (PVA) gel. J. Environ. Sci. 19, 1293–1297.
Zhao, D., Gao, X., Wu, C., Xie, R., Feng, S., Chen, C., 2016. Facile preparation of amino functionalized graphene oxide decorated with Fe_3O_4 nanoparticles for the adsorption of Cr(VI). Appl. Surf. Sci. 384, 1–9.
Zheng, S.K., Chen, J.J., Jiang, X.M., Li, X.F., 2011. A comprehensive assessment on commercially available standard anion resins for tertiary treatment of municipal wastewater. Chem. Eng. J. 169, 194–199.
Zhou, Q., Wang, X., Liu, J., Zhang, L., 2012. Phosphorus removal from wastewater using nano-particulates of hydrated ferric oxide doped activated carbon fiber prepared by Sol–Gel method. Chem. Eng. J. 200–202, 619–626.